Auger decay of Na-like $Si^{3+}(2p^5 3lnl')$ states formed in slow $Si^{5+} \rightarrow$ He and Ar ion-atom collisions

D. Schneider
Lawrence Livermore National Laboratory, P.O. Box 808, Livermore, California 94550

R. Bruch
University of Nevada–Reno, Reno, Nevada 89557

A. Shlyaptseva
Institute of Spectroscopy of the Russian Academy of Sciences, Troitsk, Moscow Region 142092, Russia

T. Brage
Computer Science Department, Vanderbilt University, Nashville, Tennessee 37235

D. Ridder
Acostas-GmbH, 8000 München 50, Germany

(Received 25 August 1994)

High-resolution autoionization spectra of multiply charged Na-like states in silicon are presented. These states have been populated in collisions of Si^{5+} ions with 50 keV impact energy on two gas targets: He and Ar. The electron emission following the decay of core-excited $2p^5 3lnl'$ ($n=3-6$) levels in Si IV has been measured. The comparison of electron spectra obtained after collisions with He and Ar is given. Theoretical Auger energies due to core-excited $(2p^5 3s^2)$, $(2p^5 3s 3p)$, $(2p^5 3p 3d)$, $(2p^5 3s 4s)$, and $(2p^5 3s 4f)$ states have been calculated relative to the $(2p^6)^1S$ limit by using the multiconfiguration Hartree-Fock method. Additional theoretical estimates of Auger transition energies originating from $(2p^5 3p^2)$, $(2p^5 3d^2)$, $(2p^5 3s 4d)$, $(2p^5 3s 5p)$, $(2p^5 3s 6s)$, $(2p^5 3s 6p)$, and $(2p^5 3s 6g)$ are also presented.

PACS number(s): 34.50.Fa, 32.80.Hd

I. INTRODUCTION

The availability of intense multiply charged ion beams at low velocities produced by electron cyclotron resonance (ECR) facilities enables detailed studies of the collision dynamics and atomic spectroscopy of highly excited ions produced by multielectron-capture processes from atomic, molecular, or surface targets. Such investigations are of fundamental importance to both basic atomic physics and applied research including technology applications. The wealth of new spectroscopic data regarding highly charged ions may help to promote a deeper understanding of high-temperature laboratory and astrophysical plasmas, relevant for fusion and x-ray laser research and plasma diagnostic in general. Within recent years the core-excited Na-like systems have been studied intensively using both Auger-electron [1–10] and optical emission spectroscopies [11–16].

In this work we present a detailed experimental and theoretical study of Na-like Auger spectra in Si IV produced in slow ion-atom collisions:

$$Si^{5+}(2p^5)+He(1s^2) \rightarrow Si^{3+}(2p^5 3lnl')+He^{2+} . \quad (1)$$

Auger electron spectroscopy using Na^+, Mg^+, Al^+, S^+, and Cl^+ projectiles interacting with Ar gas was applied by Dahl *et al.* [2] to investigate Na-like states. Some Na-like configurations, i.e., $2p^5 3s^2$, $2p^5(3s 3p\ ^3P)$, $2p^5(3s 3p\ ^1P)$, $(2p^5 3p^2\ ^3P)$, $(2p^5 3p^2\ ^1D)$, and $(2p^5 3p^2\ ^1S)$, were observed. However, the resolution was not sufficient to distinguish between individual terms and fine-structure splittings for these projectile ions.

Auger spectra of Na-like P V were observed earlier in collisions of fast phosphorous ion beams using beam-foil excitation [1]. Moreover Auger energies and decay rates for various states of the P^{4+} ion (P V) with configurations $(2p^5)3s^2, 3s 3p, 3s 3d, 3p^2, 3p 3d, 3d^2$ were calculated by Karim, Chen, and Crasemann [4]. Projectile states of the Na-like isoelectronic sequence in S VI, Cl VII, Ar VIII, Ti XII, Fe XVI, and Cu XIX were observed recently in slow [5–7] and fast [8–10] ion-atom collisions using He, Ne, and Ar as the target gas.

In addition x-ray and extreme ultraviolet (EUV) optical spectra in Na-like ions formed by dielectronic recombination processes were studied in a wide range of nuclear charge $Z=11-22$ [11,12]. These data are of importance for the creation of electron recombination EUV and x-ray lasers on the basis of Na-like systems [13–16]. A detailed theoretical analysis of L-shell Auger and radiative decays arising from the doubly excited $2p^5 3l 3l'$ states of sodium-like states was performed by Chen [17] for a wide range of ions $Z=20-90$.

In this work we focus on the identification of Si IV $(2p^5 3lnl')$ autoionizing states, in particular $2p^5 3l 3l'$ configurations. In Sec. II we describe briefly the high-resolution 0° projectile, Auger spectroscopy method applied and present some characteristic Si V Auger electron

1050-2947/95/51(6)/4652(10)/$06.00

©1995 The American Physical Society

spectra produced in 50-keV Si^{5+} collisions on He and Ar. Section III is devoted to theoretical calculations of the Si IV $(2p^5)3s^2$, $3s3p$, $3s3d$, $3p^2$, $3p3d$, $3d^2$, $3s4s$, and $3s4f$ Auger levels including fine-structure splittings. Finally, the identification of the measured Auger spectra and a discussion of the results are presented in Sec. IV.

II. EXPERIMENTAL METHOD

The high-resolution Auger electron spectra of silicon Si^{3+} (Si IV) ions presented in this paper were measured at the Lawrence Berkeley Laboratory ECR ion source at the 88-in. cyclotron. The experimental method was described in detail by Hutton, Schneider, and Prior [7]. In brief, Si^{5+} ion beams were accelerated and mass and charge analyzed by a 90° bending magnet. A second 70° magnet steered the ion beam into the atomic physics beam line. The ECR ion beam was collimated down to a 2×2-mm spot size and focused through a gas cell where the interaction with the target gas, in our case He and Ar, took place. The highly excited projectile ions following two-electron capture decay via autoionization. These autoionization electrons were separated from the ion beam by a coarse-resolution first-stage parallel-plate analyzer, which was used as an electron deflector, and a second-stage spherical high-resolution spectrometer. To minimize kinematic broadening effects, the projectile electrons were observed under 0° observation angle. A channeltron served as an electron detector. The channeltron counts were normalized with respect to the ion beam current, which was collected in a Faraday cup. Data acquisition and control of the tandem-type spectrometers and voltage sources were provided by a computer automated measurement and control (CAMAC) system. The gas cell was comprised of two coaxial cylinders electrically insulated from each other to allow electrical biasing from the ground potential. The gas in the target was regulated to a pressure as low as 1×10^{-5} Torr. The optimum pressure in the gas cell was chosen after extensive pressure-dependence studies to ensure single-collision conditions.

Figures 1(a) and 1(b) show characteristic examples of our Si L-Auger spectra arising from interactions of 50-keV Si^{5+} ions on He and Ar. The energy scale and intensities were transformed from the laboratory to the projectile emitter frame. The comparison of Figs. 1(a) and 1(b) clearly indicates that the population of specific $2p^5 3lnl'$ states differs dramatically for He and Ar as a target. A discussion of the relative line intensities is presented in Sec. IV.

In Figs. 2(a) and 2(b) we have compared a "prompt" spectrum and a time-delayed spectrum for 50-keV $Si^{5+}+He$ collisions. The spectrum in Fig. 2(b) was obtained by biasing the middle cell of the gas target, which caused a substantial shift of all autoionizing lines associated with prompt Auger transitions inside the gas cell. The corresponding lines associated with the delayed spectrum arise from projectile states, decaying after the gas cell. As can be seen, the spectra for $Si^{5+}+He$ are dominated by the $(2p^5 3s^2)^2P_{3/2,1/2}\rightarrow(2p^6\varepsilon p)^2P_{3/2,1/2}$ Coulomb allowed transitions (see Sec. IV). An interesting feature observed in this study is the different intensity ratios for the $(2p^5 3s^2)^2P_{3/2,1/2}$ line structure for the prompt and the time-delayed transitions, which deviate in both cases from the statistical ratio of 2:1.

In order to classify the observed Auger spectra we have performed detailed theoretical calculations, which are presented in the next section

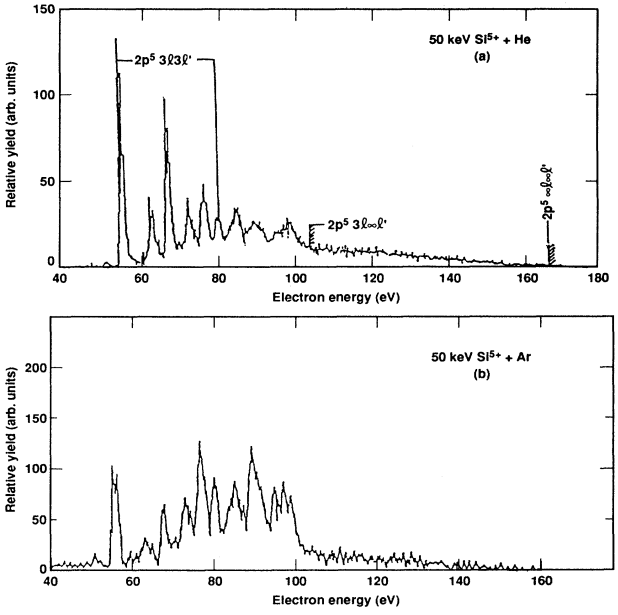

FIG. 1. Projectile Auger spectra of Si IV formed in collisions with He and Ar. The electron energies are given in the projectile frame. (a) 50-keV $Si^{5+}+He$ collisions. The $2p^5 3l\infty l'\rightarrow 2p^6\varepsilon l''$ and $2p^5 3l\infty l\infty l'\rightarrow 2p^6\varepsilon l''$ series limits and the most prominent Auger lines for the configurations in Si IV are indicated. (b) 50-keV/$Si^{5+}+Ar$ collisions.

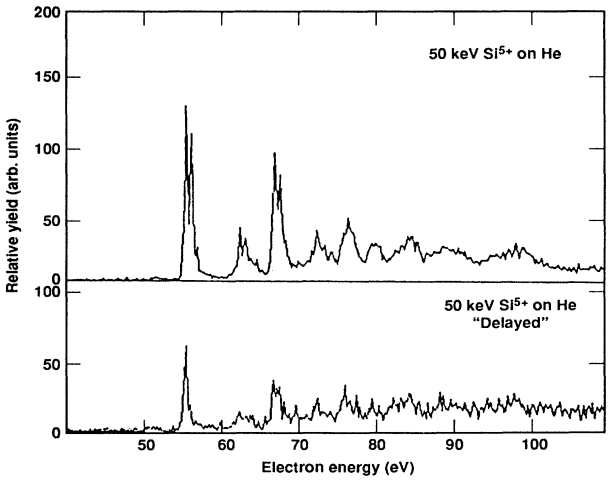

FIG. 2. Projectile L-Auger electron spectra recorded at 0° observation angle for 50-keV $Si^{5+}+He$ collisions. The upper spectrum represents prompt-decaying Auger states whereas the lower spectrum is created by time-delayed Auger transitions. The electron energies are given in the projectile frame.

III. THEORETICAL METHOD

The multiconfiguration Hartree-Fock [18] (MCHF) method has recently been used very successfully for core-excited states belonging to various isoelectronic sequences. The sodiumlike systems were studied through optical transitions between different core-excited states [19,20]. The relative position of the $2p^5 3s 3p$ and the $2p^5 3p^2$, $2p^5 3s 3d$, and $2p^5 3s 4s$ configurations was established for some long-lived states. The MCHF calculations predicted the position and lifetime of these states, in good agreement with observations. In the calculations three different decay branches were included: an optical transition between core-excited states, short wavelength, optical transitions to "normal states" (with a closed $2p^6$ core), and autoionization to the $2p^6 \varepsilon l\ ^2L$ continua. In this paper we have predicted the Auger transition energies of the core-excited states, relative to the $2p^6\ ^1S$ limit.

In the MCHF approach the atomic state function $\Psi(\alpha J)$ is represented by an expansion in configuration state functions (CSF's) $\Phi(\alpha_i L_i S_i J)$,

$$\Psi(\alpha J)=\sum_i c_i \Phi(\alpha_i L_i S_i J) \ . \tag{2}$$

The CSF's are constructed as coupled (to total L_i, S_i, and J) antisymmetric sums of products of spin orbitals $\phi(nlm_l m_s)$,

$$\phi(nlm_l m_s)=\frac{1}{r}P_{nl}(r)Y^l_{m_l}\chi(m_s) \ , \tag{3}$$

where we use the standard notation. The calculations are performed in basically two major steps: First, a variational, nonrelativistic self-consistent-field calculation of the radial functions $P_{nl}(r)$ and second, a quasirelativistic, Breit-Pauli configuration-interaction calculation to obtain the c_i coefficients. The calculations are performed separately for each configuration, so that both correlation and fine-structure effects can be represented accurately.

The first step is to obtain the core orbitals (1s, 2s, and 2p) from a Hartree-Fock calculation for the $2p^5 3s\ ^2P$ state. These are kept fixed for all states.

The $2p^6\ ^1S$ state is represented by a two-configuration-state expansion

$$c_1|2p^6\ ^1S\rangle + c_2|2p^5 3p\ ^1S\rangle \ , \tag{4}$$

where the 3p orbital and the c_i coefficients are optimized. The $2p^5 3s^2\ ^2P$ state is represented by generating all possible $2p^5 nln'l'\ ^2P$ CSFs from an active set of orbitals

$$nl, n'l' \in \{3s, 3p, 3d, 4s, 4p, 4d, 4f\} \ , \tag{5}$$

deleting some with reference to the generalized Brillouin theorem. This method is described in Refs. [21,22]. For the $2p^5 3s 3p$, $3s 3d$, $3p^2$, $3s 4s$, and $3s 4f$ configurations we

TABLE I. Theoretical values of total energies (in a.u.), energies relative to $2p^5 3s^2\ ^2P_{3/2}$ (in cm^{-1}), and Auger transition energies (in eV) relative to $2p^6\ ^1S$ for the Na-like states in Si IV.

Configuration	Level	Total energy	Energy	Auger energy
$2p^6$	$^1S_0$	−285.760 931 2	−434 850.7	0.0
$2p^5 3s^2$	$^2P_{3/2}$	−283.779 567 1	0.0	53.915
	$^2P_{1/2}$	−283.756 734 9	5 011.0	54.536
	^2P	−283.771 956		54.122
$2p^5 3s 3p\ (^3P)$	$^4S_{3/2}$	−283.566 305	46 804.7	59.718
	$^4D_{7/2}$	−283.524 906 5	55 890.4	60.845
	$^4D_{5/2}$	−283.519 981 4	56 971.4	60.979
	$^4D_{3/2}$	−283.514 581 9	58 156.4	61.126
	$^4D_{1/2}$	−283.509 564 4	59 257.6	61.262
	^4D	−283.519 830		60.983
	$^4P_{5/2}$	−283.492 664 8	62 966.6	61.722
	$^4P_{3/2}$	−283.487 358 1	64 131.2	61.866
	$^4P_{1/2}$	−283.483 369 8	65 006.5	61.975
	^4P	−283.489 347		61.812
	$^2D_{3/2}$	−283.476 956 7	66 414.0	62.149
	$^2D_{5/2}$	−283.468 950 8	68 171.1	62.367
	^2D	−283.472 153		62.280
	$^2P_{1/2}$	−283.465 712 3	68 881.8	62.455
	$^2P_{3/2}$	−283.460 207 4	70 090.0	62.605
	^2P	−283.462 042		62.555
	$^2S_{1/2}$	−283.427 861 8	77 188.9	63.485
$2p^5 3s 3p\ (^1P)$	$^2D_{5/2}$	−283.337 158 2	97 095.6	65.953
	$^2D_{3/2}$	−283.326 372 7	99 462.7	66.247
	^2D	−283.332 844		66.071

TABLE I. (*Continued*).

Configuration	Level	Total energy	Energy	Auger energy
	$^2P_{3/2}$	−283.309 357 3	103 197.1	66.710
	$^2P_{1/2}$	−283.308 441 3	103 398.1	66.735
	^2P	−283.309 052		66.718
	$^2S_{1/2}$	−283.273 623 7	111 039.6	67.682
$2p^5 3p^2(^1D)$	$^2P_{1/2}$	−283.162 901 7	135 339.8	70.695
	$^2P_{3/2}$	−283.162 296 9	135 472.5	70.712
	^2P	−283.162 498		70.706
	$^2F_{7/2}$	−283.152 308 8	137 664.6	70.983
	$^2F_{5/2}$	−283.133 458 0	141 801.8	71.496
	^2F	−283.144 230		71.203
$2p^5 3p^2(^3P)$	$^4P_{5/2}$	−283.140 350 4	140 289.1	71.309
	$^4P_{3/2}$	−283.138 119 9	140 778.6	71.370
	$^4P_{1/2}$	−283.132 135 2	142 092.1	71.532
	^4P	−283.138 238		71.366
$2p^5 3p^2(^1D)$	$^2D_{5/2}$	−283.113 719 6	146 133.8	72.033
	$^2D_{3/2}$	−283.109 950 4	146 961.0	72.136
	^2D	−283.112 212		72.074
$2p^5 3p^2(^3P)$	$^4D_{3/2}$	−283.105 949 9	147 839.0	72.245
	$^4D_{5/2}$	−283.103 165 2	148 450.2	72.321
	$^4D_{1/2}$	−283.103 107 2	148 462.9	72.322
	$^4D_{7/2}$	−283.101 200 4	148 881.4	72.374
	^4D	−283.102 930		72.327
	$^2D_{3/2}$	−283.078 654 9	153 829.5	72.988
	$^2D_{5/2}$	−283.062 128 6	157 465.5	73.437
	^2D	−283.068 739		73.257
	$^2S_{1/2}$	−283.060 730 2	157 763.4	73.475
	$^4S_{3/2}$	−283.056 631 9	158 662.8	73.587
	$^2P_{1/2}$	−283.012 591 6	168 328.4	74.785
	$^2P_{3/2}$	−283.001 983 1	170 656.6	75.074
	^2P	−283.005 519		74.978
$2p^5 3p^2(^1S)$	$^2P_{3/2}$	−282.947 599 9	182 592.1	76.554
	$^2P_{1/2}$	−282.935 754 3	185 191.9	76.876
	^2P	−282.943 651		76.661
$2p^5 3s3d(^3D)$	$^4P_{1/2}$	−283.050 864 8	159 928.5	73.744
	$^4P_{3/2}$	−283.039 147 4	162 500.2	74.063
	$^4P_{5/2}$	−283.010 722 3	168 738.7	74.836
	^4P	−283.026 888		74.396
	$^4F_{5/2}$	−283.027 887 2	164 971.5	74.369
	$^4F_{3/2}$	−283.022 958 6	166 053.1	74.503
	$^4F_{7/2}$	−283.017 223 2	167 311.9	74.659
	$^4F_{9/2}$	−282.996 485 3	171 863.2	75.224
	^4F	−283.012 921		74.776
	$^4D_{1/2}$	−283.005 817 9	169 815.0	74.970
	$^4D_{3/2}$	−282.996 490 9	171 862.0	75.223
	$^4D_{5/2}$	−282.975 801 9	176 402.6	75.786
	$^4D_{7/2}$	−282.972 901 4	177 039.2	75.865
	^4D	−282.981 781		75.624
	$^2F_{5/2}$	−282.985 549 0	174 263.4	75.521
	$^2F_{7/2}$	−282.949 930 3	182 080.7	76.490
	^2F	−282.965 196		76.075

TABLE I. (*Continued*).

Configuration	Level	Total energy	Energy	Auger energy
	$^2D_{3/2}$	−282.970 189 4	177 634.4	75.939
	$^2D_{5/2}$	−282.944 375 2	183 299.9	76.642
	^2D	−282.954 710		76.361
	$^2P_{1/2}$	−282.960 604 7	179 738.0	76.200
	$^2P_{3/2}$	−282.940 279 6	184 198.7	76.753
	^2P			76.569
$2p^5 3s 3d(^1D)$	$^2F_{7/2}$	−282.851 425 2	203 699.6	79.171
	$^2F_{5/2}$	−282.844 949 3	205 120.9	79.347
	^2F	−282.848 650		79.246
	$^2D_{3/2}$	−282.833 313 8	207 674.5	79.664
	$^2D_{5/2}$	−282.823 372 9	209 856.3	79.934
	^2D	−282.827 349		79.826
	$^2P_{1/2}$	−282.829 498 4	208 511.9	79.767
	$^2P_{3/2}$	−282.810 004 7	212 790.2	80.298
	^2P	−282.816 503		80.121
$2p^5 3s(^3P)4s$	$^4P_{5/2}$	−282.808 913 7	213 029.7	80.328
	$^4P_{3/2}$	−282.799 939 3	214 999.2	80.572
	$^4P_{1/2}$	−282.791 287 8	216 898.0	80.807
	^4P	−282.802 985		80.489
	$^2P_{3/2}$	−282.774 634 6	220 552.9	81.260
	$^2P_{1/2}$	−282.773 388 3	220 826.4	81.294
	^2P	−282.774 219		81.272
$2p^5 3s(^1P)4s$	$^2P_{3/2}$	−282.752 125 4	225 493.0	81.873
	$^2P_{1/2}$	−282.738 776 2	228 422.8	82.236
	^2P	−282.747 676		81.994

used the same technique as for Mg II [20]. This is known to be an efficient way of including both correlation and the relativistic effects.

The resulting total energies (in a.u.), energies relative to $(2p^5 3s^2)^2P_{3/2}$ (in cm^{-1}), and Auger transition energies (in eV) relative to $2p^6\,^1S$ for Na-like ($2p^5 3lnl'$) states in Si IV are listed in Table I. The sodiumlike states are similar to Li-like systems and are well known to exhibit large configuration-interaction effects. The theoretical results presented in Table I are most accurate for the relative energy of levels with an open $2p$ core, while the energy difference between the $2p^6$ and the $2p^5 3s^2$ configurations, for example, is more uncertain. When analyzing our experimental Auger spectra, accurate energy differences within the $2p^5 3s 3p$ and the $2p^5 3s^2$ configurations are of fundamental importance. The level splitting within the $2p^5 3s 3p$ configuration is expected to be correct to within a few hundred cm^{-1}. The $2p^5 3s^2$-$2p^5 3s 3p$ fine-structure doublet is probably correct to within 1000 cm^{-1}, while the $2p^6$-$2p^5 3l 3l'$ Auger energies may be off by a couple of thousand cm^{-1}.

In Table II we have tabulated results for the $2p^5 3s(^3P)4s$ and the $2p^5 3s(^1P)4s$ configurations. There are some uncertainties in the assignment of these levels, since there exists a strong interaction between these configurations and $2p^5 3p 3d$ caused by the orbitals being in the same region of space. There are also strong relativistic interactions between different terms in both configurations.

The identification of the observed Auger spectra is discussed in the next section.

IV. IDENTIFICATION OF AUGER SPECTRA AND DISCUSSION OF RESULTS

In this work the method of 0° Auger electron spectroscopy was used to study the decay of Na-like Auger states excited in slow 50-keV Si^{5+} ion-atom collisions with He and Ar target gas. The first Auger spectra of Na-like Si were observed more than 15 years ago [3], but these data were hampered by poor resolution and therefore no line identification could be given. The high-resolution Si^{5+} + He electron spectrum was reported by Hutton, Schneider, and Prior [7]; however, no line assignments were made due to a lack of theoretical data. Here we report a very detailed description and assignment of high-resolution L spectra in Si IV based on the theoretical results presented in Sec. III and additional theoretical estimates using the MCHF method [23,24]. Our experimental and theoretical findings are summarized in Table III.

TABLE II. Theoretical values of total energies (in a.u.), energies relative to $2p^3 3s^2\ ^2P_{3/2}$ (in cm^{-1}), and Auger transition energies (in eV) relative to $2p^6\ ^1S$ for the Na-like states $2p^5 3s4f$ in Si IV. The values are given by their J values and the main components in the eigenvector are given.

J	Total energy	Excitation energy	Auger energy	Eigenvector composition
1/2	−282.516 770 2	277 146.5	88.277	96.4% ^4D
3/2	−282.513 543 0	277 854.8	88.365	60.0% ^4D +31.3% ^4F
5/2	−282.508 787 6	278 898.4	84.494	37.6% ^4G +33.4% ^4F
7/2	−282.503 837 5	279 984.8	88.629	53.6% ^4G +16.1% $(^1P)^2G$
3/2	−282.500 600 3	280 695.3	88.717	40.2% ^4F +14.4% $(^1P)^2D$
5/2	−282.499 369 2	280 965.5	88.751	26.2% ^4D +20.1% $(^3P)^2D$
9/2	−282.487 903 4	283 481.9	89.063	62.6% ^4G
5/2	−282.485 967 9	283 906.7	89.115	43.2% ^4G +22.1% ^4F
3/2	−282.478 726 1	285 496.0	89.312	29.5% $(^1P)^2D$ +23.9% ^4F
7/2	−282.476 946 2	285 886.7	89.361	46.6% ^4F +17.1% $(^1P)^2G$
5/2	−282.466 459 2	288 188.3	89.646	30.2% ^4D +24.9% $(^1P)^2F$
3/2	−282.460 369 2	289 524.8	89.812	42.9% $(^3P)^2D$ +34.6% $(^1P)^2D$
11/2	−282.460 344 6	289 530.2	89.813	97.9% ^4G
7/2	−282.455 200 3	290 659.2	89.952	38.8% $(^1P)^2G$ +26.8% ^4G
5/2	−282.454 583 4	290 794.7	89.969	31.1% $(^1P)^2F$ +27.2% ^4F
9/2	−282.453 732 7	290 981.3	89.992	80.5% ^4F
7/2	−282.448 257 6	292 183.0	90.141	54.0% ^4D
5/2	−282.435 569 1	294 967.7	90.487	38.6% $(^1P)^2D$ +31.6% $(^3P)^2D$
9/2	−282.432 225 1	295 701.6	90.578	46.7% $(^3P)^2G$ +28.8% ^4G
7/2	−282.429 038 5	296 401.0	90.664	34.4% $(^3P)^2F$ +22.0% ^4F
7/2	−282.413 015 3	299 917.6	91.100	39.3% $(^3P)^2G$ +21.7% $(^1P)^2F$
5/2	−282.405 629 4	301 538.6	91.301	32.5% $(^3P)^2F$ +15.8% $3p(^1S)3d^2D$
9/2	−282.402 329 1	302 262.9	91.391	84.0% $(^1P)^2G$

TABLE III. Identification of the L-shell Auger spectrum of Si IV. An asterisk marks the most intensive experimental peaks. The $2p^5 3l3l'^1$ levels have been calculated (a) incorporating all possible $2p^5 nln'l'$ states with active $\{3s,3p,3d,4s,4p,4d,4f\}$ orbitals (Sun workstation) and (b) using reduced $\{3s,3p,3d\}$ basis sets (386 PC-AT computer). The higher $2p^5 3lnl'$ Rydberg levels represent estimates.

Peak	This work Expt. energy (eV)	Ref. [28] Calc. energy (eV) (a)	(b)	Identification of upper level	Ref. [4] P V peak intensity	Ref. [6] Fe XVI peak intensity	Ref. [10] S VI relative intensity
1*	53.915	53.915		$2p^5 3s^2\ P_{3/2}$		1	24.8*
					2*		
2*	54.536	54.536		$2p^5 3s^2\ ^2P_{1/2}$		2	11.3*
		54.122	54.05	$2p^5 3s^2\ ^2P$			
3	55.3±0.2						
4	59.7±0.2	59.718	59.86	$2p^5 3s3p(^3P)^4S_{3/2}$			
5*	61.05±0.1	60.983	61.07	$2p^5 3s3p(^3P)^4D$	$4^*_{(3/2)}$	$3^*_{(3,5,7/2)}$	
6*	61.8±0.1	61.82	61.83	$2p^5 3s3p(^3P)^4P$		$4_{(3/2)}$	
7	62.4±0.2	62.280	62.36	$2p^5 3s3p(^3P)^2D$	$7_{(3/2)}$	$4_{(5/2)}$	6.1
		62.555		$2p^5 3s3p(^3P)^2P$			8.5
8	63.3±0.2	63.485	63.69	$2p^5 3s3p(^3P)^2S_{1/2}$	6		10.6*
9	64.0±0.2						
10*	65.8±0.1	65.953		$2p^5 3s3p(^1P)^2D_{5/2}$			
					5		
11*	66.4±0.1	66.247	67.45	$2p^5 3s3p(^1P)^2D_{3/2}$			
12	66.9±0.2	66.718	67.23	$2p^5 3s3p(^1P)^2P$			
13	67.6±0.2	67.682	67.94	$2p^5 3s3p(^1P)^2S_{1/2}$	9	5	110.4*
14	68.0±0.2						
15	68.7±0.2						
16	69.9±0.2						
17	70.6±0.2	70.706	72.78	$2p^5 3p^2(^1D)^2P$	$10_{(3/2)}$	$5_{(1/2)}$	9.2
18*	71.0±0.1	70.983		$2p^5 3p^2(^1D)^2F_{7/2}$		5	

TABLE III. (*Continued*).

Peak	This work Expt. energy (eV)	Ref. [28] Calc. energy (eV) (a)	(b)	Identification of upper level	Ref. [4] P V peak intensity	Ref. [6] Fe XVI peak intensity	Ref. [10] S VI relative intensity
19	71.4±0.2	71.366		$2p^53p^2(^3P)^4P$		$5_{(5/2)}$	6.7
		71.496		$2p^53p^2(^1D)^2F_{5/2}$	10	$6_{(1/2)}$	
20	72.2±0.2	72.136		$2p^53p^2(^1D)^2D_{3/2}$		9	
		72.245		$2p^53p^2(^3P)^4D_{3/2}$		8*	
21	73.0±0.2	72.988		$2p^53p^2(^3P)^2D_{3/2}$		6	
22	73.6±0.2	73.437		$2p^53p^2(^3P)^2D_{5/2}$		9	
		73.475		$2p^53p^2(^3P)^2S_{1/2}$			
		73.587		$2p^53p^2(^3P)^4S_{3/2}$		7*	
23	74.1±0.2	74.063		$2p^53s3d(^3D)^4P_{3/2}$			
24	74.8±0.2	74.766		$2p^53s3d(^3D)^4F$		$8^*_{(7/2)}$	
		74.785		$2p^53p^2(^3P)^2P_{1/2}$	13	9.2	
		74.836		$2p^53s3d(^3D)^4P_{5/2}$		8*	
25*	75.2±0.1	75.074	79.33	$2p^53p^2(^3P)^2P_{3/2}$	13	6.7	
		75.223		$2p^53s3d(^3D)^4D_{3/2}$		10	40.1*
		75.224		$2p^53s3d(^3D)^4F_{9/2}$		8*	
26	76.0±0.2	75.865		$2p^53s3d(^3D)^4D_{7/2}$		9	
		75.939		$2p^53s3d(^3D)^2D_{3/2}$	12		40.1*
		76.075		$2p^53s3d(^3D)^2F$			
27	76.5±0.2	76.554	77.78	$2p^53p^2(^1S)^2P_{3/2}$	11*	9	
		76.569		$2p^53s3d(^3D)^2P$			$267.9^*_{(3/2)}$
		76.642		$2p^53s3d(^3D)^2D_{5/2}$	12	10	
28	78.4±0.2						
29	79.0±0.2	79.171		$2p^53s3d(^1D)^2F_{7/2}$		10	
30	79.5±0.2	79.664		$2p^53s3d(^1D)^2D_{3/2}$			95.0*
31	80.0±0.2	79.934		$2p^53s3d(^1D)^2D_{5/2}$		10	
32	80.7±0.2	80.572	80.57	$2p^53s(^3P)4s\ ^4P_{3/2}$			
		80.807		$2p^53s(^3P)4s\ ^4P_{1/2}$			
33	81.2±0.2	81.272		$2p^53s(^3P)4s\ ^2P$			
34	81.8±0.2	81.873		$2p^53s(^1P)4s\ ^2P_{3/2}$			5.4
35	82.4±0.3		82.100	$2p^53p3d(^3F)^4D$			
		82.236		$2p^53s(^1P)4s\ ^2P_{1/2}$			4.2
36	83.3±0.3		83.55	$2p^53s4p(^3P)^4S$			
37	83.7±0.3		83.80	$2p^53p3d(^1D)^2D$	$15_{(5/2)}$		
			83.87	$2p^53s4p(^3P)^4D$			
38	84.4±0.3		84.44	$2p^53s4p(^3P)^2P$			
			84.44	$2p^53s4p(^3P)^2D$			
			84.69	$2p^53p3d(^1D)^2P$			
			84.70	$2p^53s4p(^1P)^2S$			
39	85.9±0.5		85.33	$2p^53s4p(^1P)^2P$			
			85.65	$2p^53p3d(^3D)^4D$			
			86.01	$2p^53p3d(^3F)^2D$			
40	86.9±0.5		86.34	$2p^53p3d(^3P)^2P$			
			86.42	$2p^53p3d(^3P)^2S$			
			87.40	$2p^53p3d(^3P)^2D$	$16_{(3/2)}$		
			87.48	$2p^53p3d\ ^4S$			
41	88.2±0.5		88.00	$2p^53s4d(^3D)^4F$			
			88.10	$2p^53p3d(^3D)^2P$			
			88.20	$2p^53s4d(^3D)^4D$			
			88.21	$2p^53p3d(^3P)^2S$			
		88.277		$2p^53s4f\ ^4D_{1/2}$			
			88.42	$2p^53p3d(^3D)^2D$	$18_{(3,5/2)}$		
42	89.6±0.5		89.21	$2p^53s4d(^3D)^2P$			$17.5_{(3/2)}$
			89.30	$2p^53s4d(^3D)^2D$			$82.6_{(3/2)}$
		89.361		$2p^53s4f\ ^4F_{7/2}$			
		89.646		$2p^53s4f\ ^4D_{5/2}$			
		89.813		$2p^53s4f\ ^4G_{11/2}$			

TABLE III. (*Continued*).

Peak	This work Expt. energy (eV)	Ref. [28] Calc. energy (eV) (a)	(b)	Identification of upper level	Ref. [4] P V peak intensity	Ref. [6] Fe XVI peak intensity	Ref. [10] S VI relative intensity
43	91.3±0.5		90.91	$2p^5 3p 3d(^1P)^2S$			
			91.10	$2p^5 3p 3d(^1F)^2D$			
		91.301		$2p^5 3s 4f(^3P)^2F_{5/2}$			
43		91.391		$2p^5 3s 4f(^1P)^2G_{9/2}$			
			91.54	$2p^5 3s 5p(^3P)^4S$			
			91.68	$2p^5 3s 5p(^3P)^4D$			
44	94.5±0.5		94.24	$2p^5 3s 5g(^3G)^4F$			
			94.32	$2p^5 3s 5g(^1G)^2F$			
			94.35	$2p^5 3s 5g(^1G)^2G$			
			94.73	$2p^5 3s 6s(^3S)^4P$			
45	96.3±0.5		96.5	$2p^5 3s 6p(^3P)^2D$			
			96.54	$2p^5 3s 6p(^3P)^2P$			
			96.62	$2p^5 3s 6p(^3P)^2S$			
46	97.3±0.5		96.92	$2p^5 3s 6g(^3G)^4G$			
			96.99	$2p^5 3s 6g(^1G)^2H$			
			97.00	$2p^5 3s 6g(^1G)^2G$			
47	98.2±0.5		97.88	$2p^5 3s 6g(^3G)^2F$			
			97.88	$2p^5 3s 6g(^3G)^2H$			
			97.89	$2p^5 3s 6g(^3G)^2G$			
48	99.4±0.5						
49	100.9±0.5						
	103.9			$2p^5 3s\ ^3P_2 \infty l$			
	105.2			$2p^5 3s\ ^3P_1 \infty l$			
50	107.3±0.5		109.07	$2p^5 3d^2(^1D)^2P$			
51	108.8±0.5		110.41	$2p^5 3d^2(^3P)^2P$			
	136.5			$2p^5 4l \infty l'$			
	144.9			$2p^5 5l \infty l'$			
	152.9			$2p^5 6l \infty l'$			
	166.8			$2p^5 \infty l \infty l'$			

In total, 55 Auger structures have been identified and assigned to specific Auger transitions. The most dominant Auger peaks are labeled by an asterisk. In Table III we have provided a comparison of our experimental and theoretical Auger peak energies and assignment of the initial Auger states decaying to the $[2p^6\epsilon l]^2L$ continuum. Relevant additional information concerning the most characteristic experimental peaks and their relative intensities of other Na-like states in P V [4], Fe XVI [6], and S VI [10] are listed for comparison.

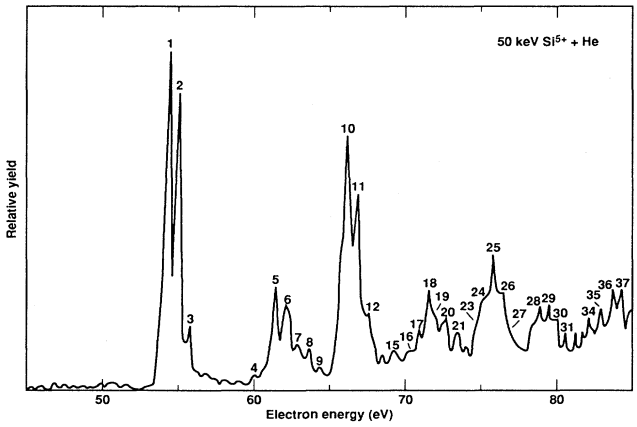

FIG. 3. Enhanced portion of the high-resolution Auger electron spectrum of Si^{3+} (Si IV) produced by 50-keV $Si^{5+}+He$ impact. The most pronounced Auger structures are labeled 1–37. The line identification is given in Table III.

In Fig. 1(a) we present an overview of the Auger electron spectrum produced in $Si^{5+}(2p^5)+He(1s^2)$ collisions. From this figure it is obvious that the dominant contributions arise from Auger decay of the $2p^5 3l 3l'$ initial states. Above the lowest series limit, namely, $(2p^5 3s)^3P_2 \infty l \rightarrow 2p^6 \epsilon l''$ at 103.9 eV (see Table III) the intensities of the observed features are very weak. According to Table III these structures stem from contributions of $(2p^5 3d^2)$ and $2p^5 nln'l'(n \geq 4,\ n' \geq 4)$ configurations. From this figure it is evident that no Auger electrons have been observed above the $2p^5 \infty l \infty l'$ limit.

An expanded segment of the high-resolution spectrum of Si IV in the energy range 40–90 eV is displayed in Fig. 3. The observed Auger line structures are labeled 1–37 and are associated with the lowest Na-like states in Si IV, namely, $(2p^5 3l 3l')$. The electron spectrum shown in this figure has been calibrated by the MCHF $(2p^5 3s^2)^2P_{3/2} \rightarrow (2p^6 \epsilon p)^2P_{3/2}$ fine-structure transition predicted at 53.915 eV. This value has been used as an

energy calibration point for all Si^{3+} spectra (see Table III). As can be seen from Fig. 3 and Table III, the most prominent fine-structure doublet, labeled 1 and 2, originates from the $(2p^5 3s^2)^2P$ $J=3/2$ and $1/2$ initial states. This fine-structure splitting has been clearly resolved in the experiment. The theoretical predictions by Brage (see Table III) are in perfect agreement with experiment. A striking result is the nonstatistical population of the $^2P_{3/2,1/2}$ levels in 50-keV $Si^{5+} \rightarrow$He collisions. The experimental intensity ratio of 1.14:1 deviates strongly from the statistical ratio of 2:1. In Table III we have listed also the corresponding relative intensities for the Auger spectrum of S VI, leading to an intensity ratio of 2:2:1, in rather good agreement with the statistical ratio.

The second prominent group of lines, labeled 5 and 6, has been identified as due to decay of the $[2p^5 3s 3p(^3P)]^4D$ and $[2p^5 3s 3p(^3P)]^4P$ metastable autoionizing states.

Another very pronounced line structure, labeled 10–13, has been identified as arising from the Auger decay of the $2p^5 3s 3p(^1P)^2D$, ^2P, and ^2S states. Peak 18 is mainly due to the $2p^5 3p^2(^1D)^2F_{7/2}$ initial state. The intense line group (25) in the vicinity of 75 eV is formed by transitions from states of both configurations: doublet terms of $2p^5 3p^2$ and $2p^5 3s 3d$. The corresponding intensities for Fe XVI are given for comparison in Table III. We further note that peaks 26 and 27 are only partially resolved and can be attributed to the $2p^5 3s 3d(^3D)^4D_{7/2}$, $^2D_{3/2}$, ^2F, $2p^5 3p^2(^1S)^2P_{3/2}$, $2p^5 3s 3d(^3D)^2P$, and $^2D_{5/2}$ upper levels. Moreover, the experimental features 29, 30, and 31 arise from the upper levels $2p^5 3s 3d(^1D)^2F_{7/2}$, $2p^5 3s 3d(^1D)^2D_{3/2}$, and $^2D_{5/2}$, respectively. There are no more intense peaks in the energy region greater than about 90 eV for Si IV [see Figs. 1(a) and 3]. Further tentative identifications of Auger transitions in the energy range from 80 to 100 eV are based in general on theoretical MCHF estimates by Ridder and some preliminary results given in Ref. [7]. The Auger transitions with energies ranging from 80 up to 90 eV are predominantly due to transitions from $2p^5 3p 3d$ and $2p^5 3s 4l$ states, where $l=s$, p, d, and f. Auger transitions with energies between 90 and 100 eV arise mainly from $2p^5 3s 6l$, with $l=s, p, d, f, g$, and h, and $2p^5 3d^2$ configurations.

When comparing the Si L-Auger spectra for He and Ar as a target gas, we have discovered fundamental differences in the observed relative peak intensities. In particular we have found that the relative intensities of the Auger transitions in the low-energy region (peaks 1, 2, and 10), corresponding to $2p^5 3s^2$ and $2p^5 3s 3p$ initial configurations, are less intense for Ar. On the other hand, the intensities of Auger peaks for Ar with higher energies (peaks 25, 37, 38, 43, and 44) are strongly enhanced when compared to the He case. We therefore conclude that the Auger lines corresponding to transitions from configurations such as $2p^5 3p^2, 2p^5 3p 3d, 2p^5 3s 4p$ and higher Rydberg states increase for 50-keV Si^{5+}+Ar collisions. This interpretation is supported by our theoretical estimates using the classical overbarrier model. Earlier it was shown [25–27] that specific outer-shell states ($n \geq 3$) are strongly populated depending systematically on the ionization potentials of the target gases. Using the classical barrier model the "principle capture quantum number" n^* produced in such electron-capture collisions and dependences of n^* on charge of projectile ions and target atoms can be analyzed. On the basis of this model we have estimated the most probable value of n^* for both collision systems with He and Ar. We have found that $n^*=3$ for collisions with He and $n^*=4$ for collisions with Ar, in accord with our experimental findings.

V. CONCLUSION

In conclusion we have identified 55 Auger structures in Si L-Auger spectra subsequent to Si^{5+}+He collisions. In particular the observed $2p^5 3l 3l'$ and $2p^5 3l 4l'$ configurations in Si IV exhibit strong electron correlation effects. Our theoretical MCHF calculations are in excellent agreement with the assigned experimental peak positions. Our spectroscopic results are of importance to unravel the details of the collision dynamics for two-electron capture in multicharged Si ions interacting with gaseous targets. For example, we have found evidence here for strong nonstatistical population of the $(2p^5 3s^2)^3P_{3/2,1/2}$ fine-structure levels in 50-keV Si^{5+}+He and Si^{5+}+Ar single collisions. This interesting process should be analyzed theoretically in the future. We also plan to extend our calculations of $2p^5 nlnl'$ states to other ions of the Na-like isoelectronic sequence.

ACKNOWLEDGMENTS

This work was performed under the auspices of the U.S. Department of Energy by the Lawrence Livermore National Laboratory under Contract No. W-7405-ENG-48. Support at LBL was obtained from the Director, Office of Energy Research, Office of Basic Energy Sciences, Chemical Sciences Division, U.S. Department of Energy under Contract No. DE-AC03-76 S F00098. One of us (A.S.) thanks ACSPECT Corp., Reno, Nevada, for partial financial support and Professor Ronald Phaneuf and his staff at Reno for their hospitality and support during the course of this work.

[1] D. Ridder and D. Schneider, Phys. Rev. A **25**, 921 (1982).
[2] P. Dahl, M. Rodbro, G. Herman, and M. E. Rudd, J. Phys. B **9**, 1581 (1976).
[3] L. Viel, C. Benazeth, and N. Benazeth, Surf. Sci. **54**, 635 (1976).
[4] K. R. Karim, M. H. Chen, and B. Crasemann, Phys. Rev. A **28**, 3355 (1983).
[5] R. Hutton, M. H. Prior, S. Chantrenne, M. H. Chen, and D. Schneider, Phys. Rev. A **39**, 4902 (1989).
[6] D. Schneider, M. Chen, S. Chatrenne, R. Hutton, and M.

H. Prior, Phys. Rev. A **40**, 4313 (1989).
[7] R. Hutton, D. Schneider, and M. H. Prior, Phys. Rev. A **44**, 243 (1991).
[8] D. Schneider, P. Beiersdorfer, M. Chen, R. Walling, J. D. Molitoris, and D. De Witt, Phys. Rev. A **40**, 181 (1989).
[9] P. Focke, T. Schneider, D. Schneider, G. Schiwietz, I. Kadar, N. Stolterfoht, and J. E. Hansen, Phys. Rev. A **40**, 5633 (1989).
[10] I. Kadar, H. Altevogt, R. Kohrbruck, V. Montemayor, A. Mattis, G. Schiwietz, B. Skogvall, K. Sommer, N. Stolterfoht, K. Kawatsura, M. Sataka, Y. Nakai, H. Naramoto, Y. Kanai, T. Kambara, Y. Awaya, K. Komaki, and Y. Yamazaki, Phys. Rev. A **44**, 2900 (1991).
[11] J. O. Gaardsted and T. Anderson, Comments At. Mol. Phys. **28**, 77 (1992).
[12] P. Bengtsson, M. Westerlind, L. Engstrom, and C. Jupen, Phys. Scr. **49**, 30 (1994).
[13] J. E. Rothenberg and S. E. Harris, IEEE J. Quantum Electron. **QE-17**, 418 (1981).
[14] D. E. Holmgren, R. W. Falcone, D. J. Walker, and S. E. Harris, Opt. Lett. **9**, 85 (1984).
[15] D. E. Holmgren, D. J. Walker, D. A. King, and S. E. Harris, Phys. Rev. A **31**, 677 (1985).
[16] S. E. Harris and J. F. Young, J. Opt. Soc. Am. B **4**, 547 (1987).
[17] M. H. Chen, Phys. Rev. A **40**, 2365 (1989).
[18] C. F. Fischer, Comput. Phys. Commun. **64**, 399 (1991).
[19] J. O. Gaardsted, T. Brage, C. F. Fischer, and D. Sonnek, Phys. Scr. **42**, 543 (1990).
[20] T. Brage and J. O. Gaardsted, Phys. Scr. **44**, 336 (1991).
[21] T. Brage and C. F. Fisher, Phys. Scr. **45**, 43 (1992).
[22] C. F. Fischer, Comput. Phys. Commun. **64**, 399 (1991).
[23] D. Ridder, Comput. Phys. Commun. **28**, 201 (1982).
[24] D. Ridder, Comput. Phys. Commun. **31**, 423 (1984).
[25] R. Mann, F. Folkmann, and H. F. Beyer, J. Phys. B **14**, 1161 (1981).
[26] M. Mack, Ph.D. thesis, University of Utrecht, The Netherlands, 1987 (unpublished).
[27] M. Mack, Nucl. Instrum. Methods B **23**, 74 (1987).
[28] D. Schneider, R. Bruch, H. Wang, T. Brage, M. H. Prior, and D. Ridder, in *VIth International Conference On The Physics of Highly Charged Ions,* edited by P. Richard, M. Stöckli, C. L. Cocke, and C. D. Lin, AIP Conf. Proc. 274 (AIP, New York, 1993), pp. 105–198.